

Journal of Materials Chemistry C

Accepted Manuscript



This is an *Accepted Manuscript*, which has been through the Royal Society of Chemistry peer review process and has been accepted for publication.

Accepted Manuscripts are published online shortly after acceptance, before technical editing, formatting and proof reading. Using this free service, authors can make their results available to the community, in citable form, before we publish the edited article. We will replace this *Accepted Manuscript* with the edited and formatted *Advance Article* as soon as it is available.

You can find more information about *Accepted Manuscripts* in the [Information for Authors](#).

Please note that technical editing may introduce minor changes to the text and/or graphics, which may alter content. The journal's standard [Terms & Conditions](#) and the [Ethical guidelines](#) still apply. In no event shall the Royal Society of Chemistry be held responsible for any errors or omissions in this *Accepted Manuscript* or any consequences arising from the use of any information it contains.

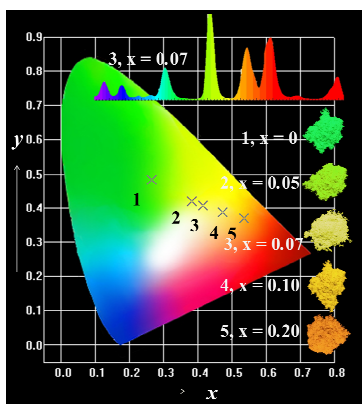
Multi-color emission evolution and energy transfer behavior of $\text{La}_3\text{GaGe}_5\text{O}_{16}:\text{Tb}^{3+},\text{Eu}^{3+}$ phosphors

Jun Zhou¹, Zhiguo Xia^{2,*}

¹*School of Materials Sciences and Technology, China University of Geosciences, Beijing 100083, China*

²*School of Materials Sciences and Engineering, University of Science and Technology Beijing, Beijing 100083, China*

Color-tunable green-red emitting $\text{La}_3\text{GaGe}_5\text{O}_{16}:\text{Tb}^{3+},\text{Eu}^{3+}$ phosphors were prepared and energy transfer process was discussed.



Multi-color emission evolution and energy transfer behavior of $\text{La}_3\text{GaGe}_5\text{O}_{16}:\text{Tb}^{3+},\text{Eu}^{3+}$ phosphors

Jun Zhou¹, Zhiguo Xia^{2,*}

¹*School of Materials Sciences and Technology, China University of Geosciences, Beijing 100083, China*

²*School of Materials Sciences and Engineering, University of Science and Technology Beijing, Beijing 100083, China*

*** Corresponding author:**

Zhiguo Xia

E-mail: xiazg@ustb.edu.cn

School of Materials Sciences and Engineering, University of Science and Technology Beijing, Beijing 100083, China

Tel. : +86-10-8237-7955;

Fax. : +86-10-8237-7955

Abstract: A series of color-tunable green-red emitting $\text{La}_3\text{GaGe}_5\text{O}_{16}:\text{Tb}^{3+},\text{Eu}^{3+}$ phosphors were prepared by a high temperature solid-state reaction, and their phase structure and photoluminescence (PL) properties were investigated in detail. A series of characteristic emission lines originated from the f-f transitions of Tb^{3+} and Eu^{3+} can be observed from the PL spectra and the emission intensities' variation of the two strong emission lines peaking at around 544 nm (green) and 617 nm (red) induced the multi-color emission evolution via the fine tuning of $\text{Tb}^{3+}/\text{Eu}^{3+}$ content ratio. The energy transfer process between Tb^{3+} and Eu^{3+} was demonstrated to be a resonant type via a dipole-dipole mechanism, and the crystal distance R_c calculated by quenching concentration method and spectral overlap method was 15.24 and 17.32 Å, respectively. Thermal quenching luminescence results reveal that $\text{La}_3\text{GaGe}_5\text{O}_{16}:\text{Tb}^{3+},\text{Eu}^{3+}$ exhibits good thermal stability.

1. Introduction

In recent years, the search for high efficiency, reliable, low power consumption and environmental friendly materials for white light-emitting diodes (*w*-LEDs) has become a proficient field. At present, there are several ways to obtain white light emission. The most common method is to employ the yellow emitting YAG:Ce phosphor and blue In GaN chips. However, such *w*-LEDs encounter low color rendering index ($R_a < 80$) and high color temperature ($T_c > 7000$ K) due to the scarcity of red emission.¹⁻² Another alternative approach to achieve white light with high R_a and suitable T_c is the combination of a UV chip with red, green, and blue phosphors. Unfortunately, the phosphor mixture produces an inevitable problem of fluorescence re-absorption between different phosphors and non-uniformity of luminescence properties, resulting in a loss of luminous efficiency and time-dependent shift of the color point.³⁻⁴ Therefore, it is urgent to develop a single-phase white-light-emitting phosphor that can be effectively excited by UV light to enhance the luminous efficiency and R_a . More importantly, compared to the multiple emitting components of the *w*-LEDs system, the single-phase white-light-emitting phosphor for a UV-pumped *w*-LEDs would also enable easy fabrication with perfect stability and color reproducibility.⁵

It is well known that the energy transfer process might be affected by the presence of carrier traps and /or defects in the host lattice. Therefore, the trace co-dopant with different affinity has potential to change the trap configuration and consequently to improve the efficiency significantly.⁶ It is clear that the Tb^{3+} acts as

a good sensitizer to enhance the luminescence efficiency of Eu^{3+} ions in $\text{Na}_3\text{Gd}(\text{PO}_4)_2$,⁷ CaYAlO_4 ,⁸ $\text{SrMg}_2\text{LaW}_2\text{O}_{12}$ ⁹ and Y_2O_3 ¹⁰ phosphors. Thus, the Tb^{3+} and Eu^{3+} ions could be used as efficient luminescent centers in practical devices. The gallogermanate of lanthanum was reported as a new mineral in 1998, and one of the chemical formula is determined as $\text{La}_3\text{GaGe}_5\text{O}_{16}$.¹¹ The crystal structure of $\text{La}_3\text{GaGe}_5\text{O}_{16}$ belongs to the triclinic system with space group $p2_1/c$, and the lattice parameters are $a = 4.827(4) \text{ \AA}$, $b = 8.090(4) \text{ \AA}$, $c = 15.707(6) \text{ \AA}$, $\alpha = 90.76(5)^\circ$, $\beta = 94.01(7)^\circ$, $\gamma = 90.01(7)^\circ$. However, to the best of our knowledge, there are no further reports on this compound and their potential optical application. In this paper, the efficient energy transfer from Tb^{3+} to Eu^{3+} in this $\text{La}_3\text{GaGe}_5\text{O}_{16}$ compound was systematically investigated by the luminescence spectra, energy transfer efficiency, and lifetime measurements. It is found that the present Tb^{3+} - Eu^{3+} codoped $\text{La}_3\text{GaGe}_5\text{O}_{16}$ phosphor will have potential applications for UV-pumped LEDs.

2. Experimental section

A series of $\text{La}_{2.85-x}\text{GaGe}_5\text{O}_{16}:0.15\text{Tb}^{3+},x\text{Eu}^{3+}$ phosphors were synthesized by high temperature solid-state reaction. Analytical reagent grade La_2O_3 (99.995%), Ga_2O_3 (99.95%), GeO_2 (99.95%), Tb_4O_7 (99.995%) and Eu_2O_3 (99.995%) were employed as raw materials, which were weighed out and mixed homogeneously by an agate mortar for 20 min and placed in an alumina crucible. This crucible was fired in air at 1250°C for 5 h and slowly cooled to room temperature.

The phase structures of the as-prepared samples were carried out on a

SHIMADZU model XRD-6000 diffractometer using Cu K α radiation ($\lambda = 0.15406$ nm) at 40 kV and 30 mA. Room temperature excitation and emission spectra were measured on a fluorescence spectrophotometer (F-4600, HITACHI, Japan) with a photomultiplier tube operating at 400 V, and a 150 W Xe lamp used as the excitation lamp. The temperature-dependence luminescence properties were measured on the same spectrophotometer, which was combined with a self-made heating attachment and a computer-controlled electric furnace. The decay curves were recorded on a spectrofluorometer (HORIBA, JOBIN YVON FL3-21), and the 370 nm pulse laser radiation (nano-LED) was used as the excitation source.

3. Results and discussion

XRD patterns of the as-prepared $\text{La}_{2.85}\text{GaGe}_5\text{O}_{16}:0.15\text{Tb}^{3+}$ and $\text{La}_{2.8}\text{GaGe}_5\text{O}_{16}:0.15\text{Tb}^{3+},0.05\text{Eu}^{3+}$ phosphors were collected to verify the phase purity. As is given in Fig. 1, one can see that all of the diffraction peaks of the samples are well indexed to the reported triclinic phase of $\text{La}_3\text{GaGe}_5\text{O}_{16}$ (JCPDS 89-0211) and no other phase is observed, indicating that the obtained samples are single phase and doped $\text{Tb}^{3+}/\text{Eu}^{3+}$ ions do not cause any significant change in the host structure. In the $\text{La}_3\text{GaGe}_5\text{O}_{16}:\text{Tb}^{3+},\text{Eu}^{3+}$ system, it is assumed that both the Eu^{3+} ($r = 0.947$ Å when coordinate number (CN) = 6 and $r = 1.066$ Å when CN = 8) ions and Tb^{3+} ($r = 0.923$ Å when CN = 6 and $r = 1.04$ Å when CN = 8) ions occupied the La^{3+} ($r = 1.16$ Å when CN = 8) sites, because both the Ga^{3+} ($r = 0.47$ Å when CN = 4) and the Ge^{4+} ($r = 0.39$ Å when CN = 4 and $r = 0.53$ Å when CN = 6) sites are too small to take the

dopant ions.

Rietveld refinements of $\text{La}_3\text{GaGe}_5\text{O}_{16}$ host was performed to further analyse the crystal structure details of the as-prepared samples. Fig. 2 demonstrates the observed, calculated, and difference patterns. It is found that $\text{La}_3\text{GaGe}_5\text{O}_{16}$ crystallized in an triclinic unit cell with space group $p2_1/c$. Furthermore, crystallographic data and details in the data collection are summarized in Table 1. As can be seen from Table 1, the obtained refinement factors are: $R_p = 2.92\%$, $R_{wp} = 3.85\%$ and $\chi^2 = 1.259$, revealing the good quality of fitting. The refined lattice parameters are $a = 4.82915(15)$ Å, $b = 8.10125(26)$ Å, $c = 15.73889(49)$ Å, and cell volume = $611.129(34)$ Å³, which match well with those reported in the literature.¹¹

Fig. 3 presents the detailed structure representation of $\text{La}_3\text{GaGe}_5\text{O}_{16}$ from y , z -projection, and different cation coordination polyhedral are shown, respectively. The basic structural units are composed of $[\text{GeO}_6]$ octahedron, $[\text{GeO}_4]$ tetrahedron and $[\text{GaO}_4]$ tetrahedron. Each $[\text{GeO}_6]$ octahedron is connected with six tetrahedron via common corners; every tetrahedron is linked to two octahedron forming chains of composition $[\text{Ge}(\text{Ga},\text{GeO}_4)_3]$ parallel $[100]$. In the b , c -plane the chains are connected by $[\text{Ge}_2\text{O}_8]$ groups which consist of two-edge-linked pseudo-tetragonal GeO_5 pyramids to a three dimensional framework structure with channels parallel $[100]$.¹¹

Fig. 4a shows the PLE and PL spectra of $\text{La}_{2.85}\text{GaGe}_5\text{O}_{16}:0.15\text{Tb}^{3+}$. The PLE spectrum is recorded by monitoring with bright green emission ($^5\text{D}_4$ - $^7\text{F}_5$) at 544 nm, which reveals a series of spectral bands in the range of 300 nm to 400 nm. The electronic transitions of Tb^{3+} have been appropriately designated as $^7\text{F}_6$ - $^5\text{H}_6$ at 303 nm,

7F_6 - 5H_7 at 317 nm, 7F_6 - 5D_2 at 340 and 351 nm, and 7F_6 - 5G_6 at 369 and 377 nm. Of these excitation peaks, the most prominent peak at 377 nm is chosen to pump for which strong emission is observed at 544 nm besides other emission spectral lines in the blue and green regions. The spectral lines in the blue region are found to be at 417 nm (5D_3 - 7F_5) and 440 nm (5D_3 - 7F_4) with very low intensity. The peaks arising in the green region at 491 nm, 544 nm, 585 nm, and 624 nm are assigned to 5D_4 - ${}^7F_{J=6,5,4,3}$ transitions, respectively. In agreement with the magnetic dipole transition selection rule $\Delta J = \pm 1$, Laporte's forbidden transition 5D_4 - 7F_5 (544 nm) showed bright green luminescence compared with the other emission transitions measured.¹² Of these peaks, the green emission at 544 nm has the strongest intensity and largest probability for electric-dipole transition.

Fig. 4b represents the PLE and PL spectra of $\text{La}_{2.95}\text{GaGe}_5\text{O}_{16}:0.05\text{Eu}^{3+}$. The PLE spectrum monitored at 617 nm shows a broad band and sharp peaks in the range of 300-500 nm, which are attributed to the 4f-4f transitions within Eu^{3+} $4f^6$ electron configuration. It is a good sign that this phosphor can strongly absorb ultraviolet (396 nm). The wavelength is nicely in agreement with the widely applied output wavelengths of UV LED chips.¹³ Upon the excitation of 396 nm, the figure displayed two groups of PL bands corresponding to the 5D_1 - ${}^7F_{1,2}$ and 5D_0 - 7F_J ($J = 0, 1, 2, 3, 4$) transitions. In case of Eu^{3+} , the 5D_1 - ${}^7F_{1,2}$ emission transitions are insignificant and the 5D_0 - ${}^7F_{0,1,2,3,4}$ transitions with peak maxima at 583, 596, 617, 656 and 701 nm, respectively are noteworthy. A significant spectral overlap is observed by comparing the excitation band of $\text{La}_{2.95}\text{GaGe}_5\text{O}_{16}:0.05\text{Eu}^{3+}$ with the emission band of

$\text{La}_{2.85}\text{GaGe}_5\text{O}_{16}:0.15\text{Tb}^{3+}$, which is in favor of the resonance type energy transfer from Tb^{3+} to Eu^{3+} .

Fig. 4c illustrates the PLE and PL spectra of the typical $\text{La}_{2.8}\text{GaGe}_5\text{O}_{16}:0.15\text{Tb}^{3+},0.05\text{Eu}^{3+}$. The excitation spectra which irradiated wave-length of 617 nm and 544 nm were identical to that of Tb^{3+} singly doped phosphor, which shows that doubly doped $\text{La}_3\text{GaGe}_5\text{O}_{16}$ can be used as green and red double-color-emitting phosphors in near UV-pumped white LEDs. On the other hand, the emission peaks of the Eu^{3+} , Tb^{3+} codoped phosphor under 377 nm excitation were observed at 617 nm and 544 nm, attributed to the Eu^{3+} and Tb^{3+} ion, respectively. Therefore, the relative intensities of these two emissions can be varied by adjusting the concentrations of the two activators through the principle of energy transfer.

In order to understand the energy transfer process, a series of composition-controlled samples were prepared. **Fig. 5** illustrates the dependence of PL spectra for Tb^{3+} and Eu^{3+} co-doped $\text{La}_{2.85-x}\text{GaGe}_5\text{O}_{16}:0.15\text{Tb}^{3+},x\text{Eu}^{3+}$ phosphors. Under excitation with 377 nm UV light, the characteristic sharp emission of Tb^{3+} as well as sharp emission peaks of Eu^{3+} are observed in emission spectra. With increasing Eu^{3+} content, the emission intensities of the Eu^{3+} at 596 and 617 nm increased systematically whereas the emission intensities of the Tb^{3+} ions simultaneously decreased, reflecting the result of energy transfer from Tb^{3+} to Eu^{3+} .

To observe directly the relative emission intensity variation, the intensities of Tb^{3+} and Eu^{3+} emissions are given in **Fig. 6** as a function of the Eu^{3+} content. The

observed variations in the Tb^{3+} and Eu^{3+} emissions curves further support the occurrence of the effective energy transfer from the Tb^{3+} to Eu^{3+} ions. Therefore, the Tb^{3+} to Eu^{3+} energy transfer efficiency (η_T) in the $\text{La}_3\text{GaGe}_5\text{O}_{16}$ host can be expressed as¹⁴

$$\eta_T = 1 - \frac{I_S}{I_{S0}} \quad (1)$$

where I_{S0} is the luminescence intensities of the sensitizer Tb^{3+} in the sample in the absence of Eu^{3+} , and I_S is the luminescence intensities of Tb^{3+} in the presence of Eu^{3+} . The dependence of η_T on the Eu^{3+} doping concentration is shown in Fig. 6. It is clearly observed that the value of η_T gradually increases with increasing Eu^{3+} concentration. The maximum η_T value is determined to be as high as 87.12% for $\text{La}_{2.65}\text{GaGe}_5\text{O}_{16}:0.15\text{Tb}^{3+},0.20\text{Eu}^{3+}$ phosphor.

In general, the resonant-type energy transfer from a sensitizer to an activator in a phosphor may take place via the exchange interaction and electric multipolar interaction.¹⁵ It is known that if energy transfer takes the exchange interaction, the critical distance between the sensitizer and activator should be shorter than 3-4 Å.¹⁶ The critical distance R_C for energy transfer from the Tb^{3+} to Eu^{3+} ions was calculated using the concentration quenching method. The critical distance R_C between Tb^{3+} and Eu^{3+} can be estimated by the following formula suggested by Blasse:¹⁷

$$R_C \approx 2 \left[\frac{3V}{4\pi x_c N} \right]^{1/3} \quad (2)$$

here N is the number of molecules in the unit cell, V is the unit cell volume and x_c is the critical concentration. For $\text{La}_3\text{GaGe}_5\text{O}_{16}$ host, $N = 2$, $V = 611.81 \text{ \AA}^3$ and the critical concentration is about 0.165 from the total concentration of Tb^{3+} and Eu^{3+} at which

the energy transfer efficiency is 0.5. According to the above equation, the critical distance of energy transfer is estimated to be about 15.24 Å. This value is much longer than 3-4 Å, indicating little possibility of energy transfer via the exchange interaction mechanism. Thus, energy transfer mechanism in this system is governed by the electric multipolar interaction.

The energy transfer mechanism for multipolar interactions has been discussed by many authors and can be determined using the relation:¹⁸⁻¹⁹

$$\eta_0 / \eta \propto C^{n/3} \quad (3)$$

In which η_0 and η are the luminescence quantum efficiencies of Tb^{3+} in the absence and presence of Eu^{3+} , respectively; the values of η_0 / η_s can be approximately calculated by the ratio of related luminescence intensities (I_{so} / I_s); C is the concentration of the sum of Tb^{3+} and Eu^{3+} ; and the $n = 6, 8,$ and $10,$ are dipole-dipole, dipole-quadrupole, and quadrupole-quadrupole interactions. The I_{so}/I_s plots are illustrated in Fig. 7 for $\text{La}_{2.85-x}\text{GaGe}_5\text{O}_{16}:0.15\text{Tb}^{3+},x\text{Eu}^{3+}$ phosphors, and the relationships are tested when $n = 6, 8,$ and $10.$ The linear behavior was observed only when $n = 6,$ implying that energy transfer from Tb^{3+} to Eu^{3+} occurs via a dipole-dipole mechanism.

Therefore, according to dipole-dipole interaction mechanism, R_C can be obtained from the following simplified equation:²⁰

$$R_c^6 = (3 \times 10^{12}) f_d \int \frac{F_s(E)F_A(E)}{E^4} \quad (4)$$

Where $f_d \approx 0.02$ is the electric dipole oscillator strength for Eu^{3+} ions, E is the energy involved in the transfer (in eV), and $\int F_s(E)F_A(E)/E^4 dE$ represents the spectral overlap between the normalized shapes of Tb^{3+} emission $F_s(E)$ and Eu^{3+} excitation $F_A(E).$ Using the above equation, the R_C of the energy transfer was

estimated to be about 17.32 Å, which agrees approximately with the data that obtained by using concentration quenching method (15.24 Å). This result further reveals that the mechanism of the energy transfer the Tb³⁺ to Eu³⁺ is mainly due to a dipole-dipole interaction.

In order to further demonstrate the energy transfer from Tb³⁺ to Eu³⁺, the decay curves of Tb³⁺ emission of La_{2.85-x}GaGe₅O₁₆:0.15Tb³⁺,_xEu³⁺ ($x = 0, 0.01, 0.05, 0.10, 0.20$) excited at 377 nm and monitored at 544 nm are shown in Fig. 8. It was found that all decay curves can be well fitted by the first order exponential decay method using the formula:²¹⁻²²

$$I(t) = I_0 \exp(-t/\tau) \quad (5)$$

Where $I(t)$ and I_0 are the luminescence intensities at time t and 0, and τ is the radiative decay time. On the basis of equation, the effective lifetime values were calculated to be 2.98, 2.16, 1.55, 0.95 and 0.81 ms for La_{2.85-x}GaGe₅O₁₆:0.15Tb³⁺,_xEu³⁺ with $x = 0, 0.01, 0.05, 0.10$ and 0.20, respectively. We can see that the decay lifetime of the Tb³⁺ ions decreases monotonically with the Eu³⁺ concentration increasing, which can further confirm the existence of energy transfer from Tb³⁺ to Eu³⁺ ions. Therefore, the energy transfer efficiency from Tb³⁺ to Eu³⁺ can be calculated based on the following expression:²³

$$\eta_T = 1 - \frac{\tau_x}{\tau_0} \quad (6)$$

here τ_0 and τ_x are the corresponding lifetimes of donor Tb³⁺ in the absence and the presence of the acceptor Eu³⁺, and η_T is the calculation of energy transfer efficiency. It can be seen from Fig. 8 that the energy transfer efficiency (η_T) increases with increasing Eu³⁺ concentration. The η_T value is estimated to be 72.82% when the concentration of Eu³⁺ is up to 0.2 mol, which is in good agreement with that obtained

above (87.12%).

The thermal quenching of phosphors applied in WLEDs is one of the most important technological parameters because it has great influence on the light output and CRI. Thus, temperature-dependent relative emission intensities under 377 nm excitation of as-prepared $\text{La}_{2.8}\text{GaGe}_5\text{O}_{16}:0.15\text{Tb}^{3+},0.05\text{Eu}^{3+}$ are indicated in Fig. 9. And the variations of the relative emission intensities (a) and CIE chromaticity coordinates (b) as a function of temperature are displayed in Fig. 10. As can be seen in Fig. 10(a), when the temperature was increased to 150 °C, the PL intensities of Tb^{3+} and Eu^{3+} ions are decreased to 92.2% and 89.1% of the corresponding initial value (25 °C), while the emission intensity of the commercial $\text{Ba}_2\text{SiO}_4:\text{Eu}^{2+}$ phosphor decreases to 77.8%. The fair thermal stability, compared with commercial phosphor, demonstrated that $\text{La}_3\text{GaGe}_5\text{O}_{16}:\text{Tb}^{3+},\text{Eu}^{3+}$ phosphor could be potential for high-powered LED applications. Generally, the thermal quenching of emission intensity can be explained by the temperature dependence of the electron-phonon interactions in the luminescence center and thermally activated photo-ionization of lanthanide. These two mechanisms are strongly related to the crystal structure of host lattices and crystallinity of the phosphors, and are based on the observed thermal quenching rates.²⁴ Additionally, the $\text{Tb}^{3+}/\text{Eu}^{3+}$ intensity ratio of $\text{La}_{2.8}\text{GaGe}_5\text{O}_{16}:0.15\text{Tb}^{3+},0.05\text{Eu}^{3+}$ increases and CIE chromaticity coordinates shift to green region with increasing temperature, as shown in Fig. 10(b). However, the emission colors from 25 °C to 250 °C still located in a small region, as given in the dotted red circles in the CIE diagram. Moreover, we have also compared the emission intensities between as-prepared $\text{La}_{2.85}\text{GaGe}_5\text{O}_{16}:0.15\text{Tb}^{3+}$ and commercial green $\text{Ba}_2\text{SiO}_4:\text{Eu}^{2+}$ phosphor. As can be seen in Fig. 11, the intensity of $\text{La}_{2.85}\text{GaGe}_5\text{O}_{16}:0.15\text{Tb}^{3+}$ is inferior to that of commercial $\text{Ba}_2\text{SiO}_4:\text{Eu}^{2+}$, which

should be ascribed to the sharp-line f-f transition of Tb^{3+} . However, such a green emission will induce the better color purity in some potential applications.

Furthermore, to further verify the origin of temperature-dependent emission intensity (I_T), the activation energy (ΔE) was calculated using the Arrhenius equation:²⁵⁻²⁶

$$I_T = \frac{I_0}{1 + c \exp\left(-\frac{\Delta E}{kT}\right)} \quad (7)$$

where I_0 is the initial PL intensity of the phosphor at room temperature, I_T is the PL intensity at different temperatures, c is a constant, ΔE is the activation energy for thermal quenching, and k is Boltzmann constant ($8.62 \times 10^{-5} \text{eV}$). According to the equation, the activation energy ΔE can be calculated from a plotting of $\ln[(I_0/I)-1]$ against $1/kT$, where a straight slope equals $-\Delta E$. As shown in Fig. 12, ΔE were found to be 0.449 and 0.345 eV for Tb^{3+} and Eu^{3+} , respectively. The relatively high activation energy results in a good thermal stability for this phosphor.

The x and y values of CIE chromaticity coordinates for $\text{La}_{2.85-x}\text{GaGe}_5\text{O}_{16}:0.15\text{Tb}^{3+},x\text{Eu}^{3+}$ with different dopant contents were measured and presented in Fig. 13 and Table 2, respectively. The color tone can tuned from green (0.2643, 0.4813) to red (0.5345, 0.3694) by doping different concentrations of Eu^{3+} ions. As also given in the photographs of the emitting phosphors, the as-observed emitting color is obvious, which means that the tunable luminescence can be realized in the novel $\text{La}_{2.85-x}\text{GaGe}_5\text{O}_{16}:0.15\text{Tb}^{3+},x\text{Eu}^{3+}$ phosphors based on energy transfer.

4. Conclusion

In summary, we have successfully synthesized a series of color-tunable

$\text{La}_3\text{GaGe}_5\text{O}_{16}:\text{Tb}^{3+},\text{Eu}^{3+}$ phosphors and investigated their luminescence properties. The luminescence spectra and fluorescence decay curves indicate that there is an efficient energy transfer from Tb^{3+} to Eu^{3+} ions via a dipole-dipole mechanism. And the critical distance was calculated by both the concentrating quenching and spectral overlap methods. Because of the energy transfer, the emission color of the obtained phosphors can be varied from green (0.2643, 0.4813) to red (0.5345, 0.3694) by adjusting the concentration of Eu^{3+} . Moreover, the temperature dependence of luminescence shows this phosphor has an excellent thermal stability on the temperature quenching. These results indicate that $\text{La}_3\text{GaGe}_5\text{O}_{16}:\text{Tb}^{3+},\text{Eu}^{3+}$ can be promising as a potential candidate for the application in white LEDs.

Acknowledgements

The present work was supported by the National Natural Science Foundations of China (Grant No. No.51002146, No.51272242), Natural Science Foundations of Beijing (2132050), the Program for New Century Excellent Talents in University of Ministry of Education of China (NCET-12-0950), Beijing Nova Program (Z131103000413047), Beijing Youth Excellent Talent Program (YETP0635) and the Funds of the State Key Laboratory of New Ceramics and Fine Processing, Tsinghua University (KF201306). Z. G. Xia also thanks for the financial support from University of Science and Technology Beijing.

References

- 1 P. Schlotter, R. Schmidt and J. Schneider, *Appl. Phys. A*, 1997, **64**, 417.
- 2 V. Bachmann, C. Ronda and A. Meijerink, *Chem. Mater.*, 2009, **21**, 2077.

- 3 N. Toshio, B. Tomoyuki and N. Kobayashi, *Appl. Phys. Lett.*, 2009, **82**, 3817.
- 4 Y. Liu, X. Zhang, Z. Hao, X. Wang and J. Zhang, *Chem. Commun.*, 2011, **47**, 10677.
- 5 Z. G. Xia and R. S. Liu, *J. Phys. Chem. C*, 2012, **116**, 15604.
- 6 H. Yamamoto and K. Urade, *J. Electrochem. Soc.*, 1982, **129**, 2069.
- 7 D. Wang, Y. Wang and J. W. He, *Mater. Res. Bull.*, 2012, **47**, 142.
- 8 D. Q. Geng, G. G. Li, M. M. Shang, C. Peng, Y. Zhang, Z. Y. Cheng and J. Lin, *Dalton. Trans.*, 2012, **41**, 3078.
- 9 K. Pavani, J. Suresh Kumar and L. Rama Moorthy, *J. Alloys. Compd.*, 2014, **586**, 722.
- 10 M. Back, M. Boffelli, A. Massari, R. Marin, F. Enrichi and P. Riello, *J. Nanopart. Res.*, 2013, **15**, 1753.
- 11 G. Adiwidjaja, M. Broker, C. Claus, K. Friese, K. H. Klaska, O. Jarchow, M. Ruks and I. Wozniak, *Z. Kristallogr.*, 1998, **213**, 223.
- 12 V. Naresh and S. Buddhudu, *J. Lumin.*, 2013, **137**, 15.
- 13 I. Akasaki and H. Amano, *Jpn. J. Appl. Phys.*, 1997, **36**, 5393.
- 14 P. I. Paulose, G. Jose, V. Thomas, N. V. Unnikrishnan and M. K. R. Warriar, *J. Phys. Chem. Solids.*, 2003, **64**, 841.
- 15 R. Reisfeld, E. Greenberg, R. Velapoldi and B. Barnett, *J. Chem. Phys.*, 1972, **56**, 1698.
- 16 B. M. Antipeuko, I. M. Bataev, V. L. Ermolaev, E. I. Lyubimov and T. A. Privalova, *Opt. Spectrosc.*, 1970, **29**, 177.
- 17 G. Blasse, *J. Solid State Chem.*, 1986, **62**, 207.
- 18 H. Jiao, F. Liao, S. Tian and X. J. Jing, *J. Electrochem. Soc.*, 2003, **150**, H220.

- 19 D. L. Dexter and J. A. Schulman, *J. Chem. Phys.*, 1954, **22**, 1063.
- 20 D. L. Dexter, *J. Chem. Phys.*, 1953, **21**, 836.
- 21 Z. G. Xia, J. Q. Zhuang, A. Meijerink and X. P. Jing, *Dalton. Trans.*, 2013, **42**, 6327.
- 22 J. Hao, S. A. Studenikin and M. Cocivera, *J. Appl. Phys.*, 2001, **90**, 5064.
- 23 P. I. Paulose, G. Jose, V. Thomas, N. V. Unnikrishnan and M. K. R. Warriar, Cocivera, *J. Phys. Chem. Solids.*, 2003, **64**, 841.
- 24 H. D. Luo, J. Liu, X. Zheng, L. X. Han, K. X. Ren and X. B. Yu, *J. Mater. Chem.*, 2012, **22**, 15892.
- 25 J. Zhou, Z. G. Xia, M. X. Yang and K. Shen, *J. Mater. Chem.*, 2012, **22**, 21935.
- 26 Z. G. Xia, R. S. Liu, K. W. Huang and V. Droid, *J. Mater. Chem.*, 2012, **22**, 15183.

The table and figure captions are as follows,

Table. 1 Main crystallographic parameters for $\text{La}_3\text{GaGe}_5\text{O}_{16}$ from the GSAS Rietveld Refinement.

Table. 2 CIE chromaticity coordinates (x, y) for $\text{La}_{2.85-x}\text{GaGe}_5\text{O}_{16}:0.15\text{Tb}^{3+},x\text{Eu}^{3+}$ ($x = 0, 0.05, 0.07, 0.10, 0.20$) samples ($\lambda_{\text{ex}} = 377 \text{ nm}$).

Fig. 1 XRD patterns of as-prepared $\text{La}_{2.85}\text{GaGe}_5\text{O}_{16}:0.15\text{Tb}^{3+}$ (a), and $\text{La}_{2.8}\text{GaGe}_5\text{O}_{16}:0.15\text{Tb}^{3+},0.05\text{Eu}^{3+}$ (b) phosphors. The standard data for $\text{La}_3\text{GaGe}_5\text{O}_{16}$ (JCPDS card no. 89-0211) is shown as a reference.

Fig. 2 Powder XRD patterns for Rietveld structure analysis of the selected $\text{La}_3\text{GaGe}_5\text{O}_{16}$. The solid red lines are calculated intensities, and the crosses are the observed intensities. The short vertical lines show the position of Bragg reflections of the calculated pattern. The blue solid lines below the profiles stand for the difference between the observed and calculated intensities. The inset shows the crystal structure of $\text{La}_3\text{GaGe}_5\text{O}_{16}$ sample.

Fig. 3 View of the structure of $\text{La}_3\text{GaGe}_5\text{O}_{16}$ from y, z -projection, and different cation coordination polyhedral are shown, respectively.

Fig. 4 PLE and PL spectra of $\text{La}_{2.85}\text{GaGe}_5\text{O}_{16}:0.15\text{Tb}^{3+}$ (a), $\text{La}_{2.95}\text{GaGe}_5\text{O}_{16}:0.05\text{Eu}^{3+}$ (b), and $\text{La}_{2.8}\text{GaGe}_5\text{O}_{16}:0.15\text{Tb}^{3+},0.05\text{Eu}^{3+}$ (c) phosphors.

Fig. 5 PL spectra of $\text{La}_{2.85-x}\text{GaGe}_5\text{O}_{16}:0.15\text{Tb}^{3+},x\text{Eu}^{3+}$ phosphors as a function of Eu^{3+} doping content (x).

Fig. 6 Variation of the Eu^{3+} concentration for the Eu^{3+} emission, Tb^{3+} emission and energy transfer efficiency of $\text{Tb}^{3+}-\text{Eu}^{3+}$ in $\text{La}_{2.85-x}\text{GaGe}_5\text{O}_{16}:0.15\text{Tb}^{3+},x\text{Eu}^{3+}$ phosphors.

Fig. 7 Dependence of I_{S0}/I_S of Tb^{3+} on (a) $C_{(Tb^{3+}+Eu^{3+})}^{6/3}$, (b) $C_{(Tb^{3+}+Eu^{3+})}^{8/3}$ and (c) $C_{(Tb^{3+}+Eu^{3+})}^{10/3}$.

Fig. 8 Decay curves and lifetime of Tb^{3+} , and the energy transfer efficiency from Tb^{3+} to Eu^{3+} in $La_{2.85-x}GaGe_5O_{16}:0.15Tb^{3+},xEu^{3+}$ ($x = 0, 0.01, 0.05, 0.10, 0.20$) phosphors at room temperature.

Fig. 9 Temperature-dependent PL spectra of $La_{2.8}GaGe_5O_{16}:0.15Tb^{3+},0.05Eu^{3+}$ under different temperatures in the range of 25-250°C.

Fig. 10 The variations of the relative emission intensities (a) and CIE chromaticity coordinates (b) as a function of temperature of the $La_{2.8}GaGe_5O_{16}:0.15Tb^{3+},0.05Eu^{3+}$ phosphor.

Fig. 11 PL spectra of $La_{2.85}GaGe_5O_{16}:0.15Tb^{3+}$ phosphor and commercial $Ba_2SiO_4:Eu^{2+}$ phosphors.

Fig. 12 A $\ln[(I_0/I_T)-1]$ vs. $1/K_B T$ activation energy graph for thermal quenching of Tb^{3+} and Eu^{3+} in $La_{2.8}GaGe_5O_{16}:0.15Tb^{3+},0.05Eu^{3+}$ phosphor.

Fig. 13 CIE chromaticity diagram and a series of digital photographs of the selected of the $La_{2.85-x}GaGe_5O_{16}:0.15Tb^{3+},xEu^{3+}$ ($x = 0, 0.05, 0.07, 0.10, 0.20$) phosphors under 377 nm excitation. The inset shows the PL spectrum of $La_{2.79}GaGe_5O_{16}:0.15Tb^{3+},0.07Eu^{3+}$ under 377nm UV light excitation.

Table. 1 Main crystallographic parameters for $\text{La}_3\text{GaGe}_5\text{O}_{16}$ from the GSAS Rietveld Refinement.

Formula	$\text{La}_3\text{GaGe}_5\text{O}_{16}$	ICSD-50521- $\text{La}_3\text{GaGe}_5\text{O}_{16}$
crystal system		triclinic
space group		$p2_1/c$
2θ -interval, °		10-80
α , °	90.6620(17)	90.76(5)
β , °	94.0919(17)	94.01(7)
γ , °	89.9710(17)	90.01(7)
a (Å)	4.82915(15)	4.827(4)
b (Å)	8.10125(26)	8.090(4)
c (Å)	15.73889(49)	15.707(6)
V (Å ³)	611.129(34)	611.81(310)
Z		2
R_{wp} (%)	3.85	-
R_{p} (%)	2.92	-
χ^2	1.259	-

Table. 2 CIE chromaticity coordinates (x, y) for $\text{La}_{2.85-x}\text{GaGe}_5\text{O}_{16}:0.15\text{Tb}^{3+},x\text{Eu}^{3+}$ ($x = 0, 0.05, 0.07, 0.10, 0.20$) samples ($\lambda_{\text{ex}} = 377 \text{ nm}$).

Sample NO.	Sample composition (x)	CIE coordinates (x, y)
1	0	(0.2643, 0.4813)
2	0.05	(0.3832, 0.4199)
3	0.07	(0.4156, 0.4085)
4	0.10	(0.4718, 0.3880)
5	0.20	(0.5345, 0.3694)

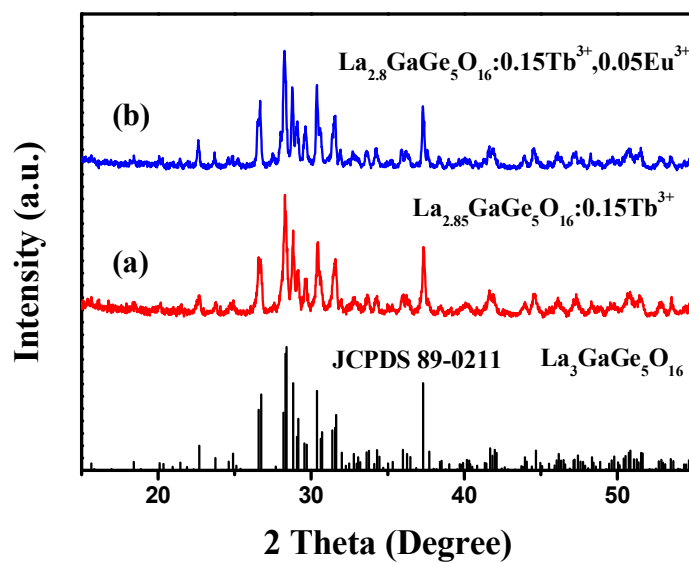


Fig. 1 XRD patterns of as-prepared $\text{La}_{2.85}\text{GaGe}_5\text{O}_{16}:0.15\text{Tb}^{3+}$ (a), and $\text{La}_{2.8}\text{GaGe}_5\text{O}_{16}:0.15\text{Tb}^{3+}, 0.05\text{Eu}^{3+}$ (b) phosphors. The standard data for $\text{La}_3\text{GaGe}_5\text{O}_{16}$ (JCPDS card no. 89-0211) is shown as a reference.

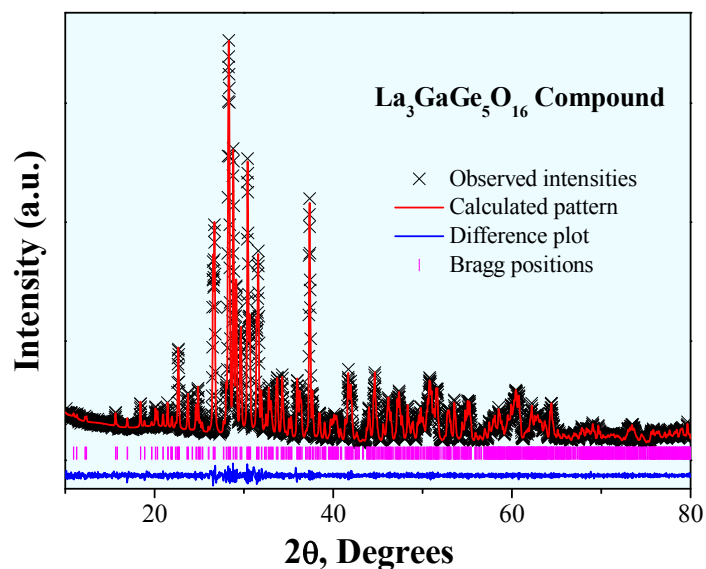


Fig. 2 Powder XRD patterns for Rietveld structure analysis of the selected $\text{La}_3\text{GaGe}_5\text{O}_{16}$. The solid red lines are calculated intensities, and the crosses are the observed intensities. The short vertical lines show the position of Bragg reflections of the calculated pattern. The blue solid lines below the profiles stand for the difference between the observed and calculated intensities.

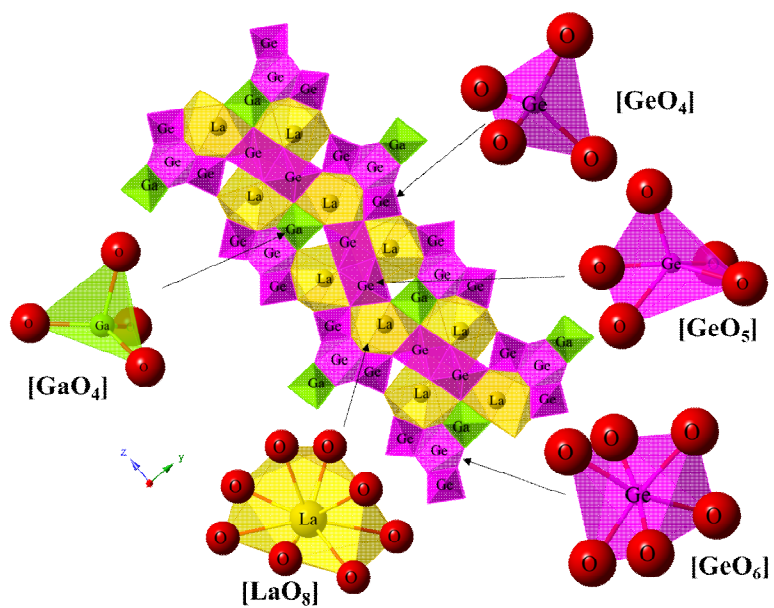


Fig. 3 View of the structure of $\text{La}_3\text{GaGe}_5\text{O}_{16}$ from y, z -projection, and different cation coordination polyhedra are shown, respectively.

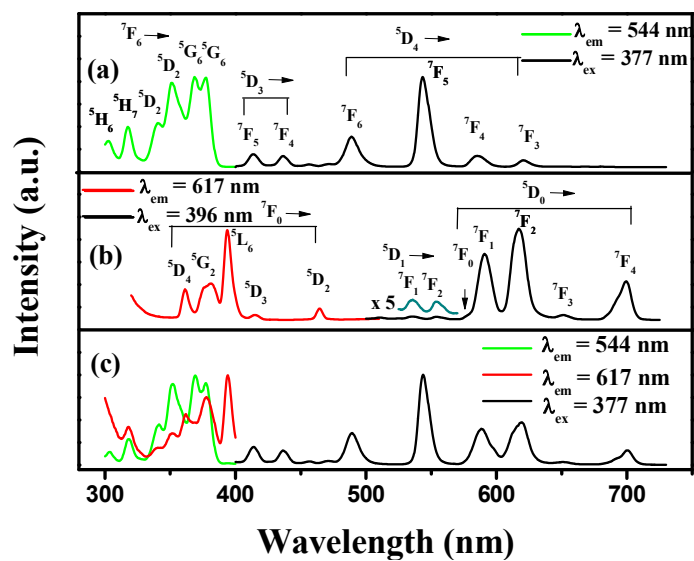


Fig. 4 PLE and PL spectra of $\text{La}_{2.85}\text{GaGe}_5\text{O}_{16}:0.15\text{Tb}^{3+}$ (a), $\text{La}_{2.95}\text{GaGe}_5\text{O}_{16}:0.05\text{Eu}^{3+}$ (b), and $\text{La}_{2.8}\text{GaGe}_5\text{O}_{16}:0.15\text{Tb}^{3+}, 0.05\text{Eu}^{3+}$ (c) phosphors.

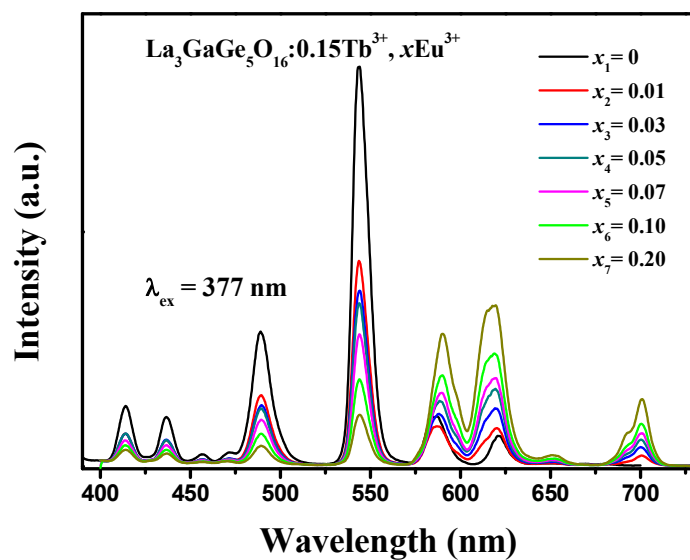


Fig. 5 PL spectra of $\text{La}_{2.85-x}\text{GaGe}_5\text{O}_{16}:0.15\text{Tb}^{3+}, x\text{Eu}^{3+}$ phosphors as a function of Eu^{3+} doping content (x).

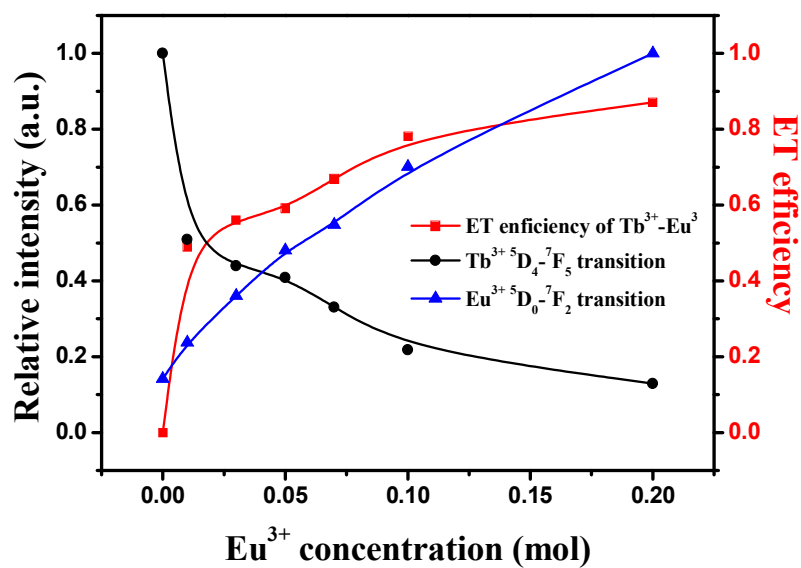


Fig. 6 Variation of the Eu³⁺ concentration for the Eu³⁺ emission, Tb³⁺ emission and energy transfer efficiency of Tb³⁺-Eu³⁺ in La_{2.85-x}GaGe₅O₁₆:0.15Tb³⁺,_xEu³⁺ phosphors.

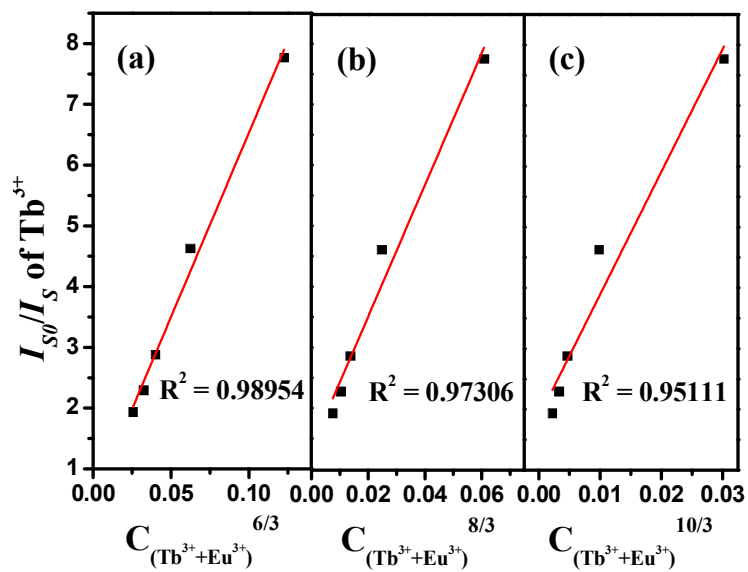


Fig. 7 Dependence of I_{S0}/I_S of Tb^{3+} on (a) $C_{(Tb^{3+}+Eu^{3+})}^{6/3}$, (b) $C_{(Tb^{3+}+Eu^{3+})}^{8/3}$ and (c) $C_{(Tb^{3+}+Eu^{3+})}^{10/3}$.

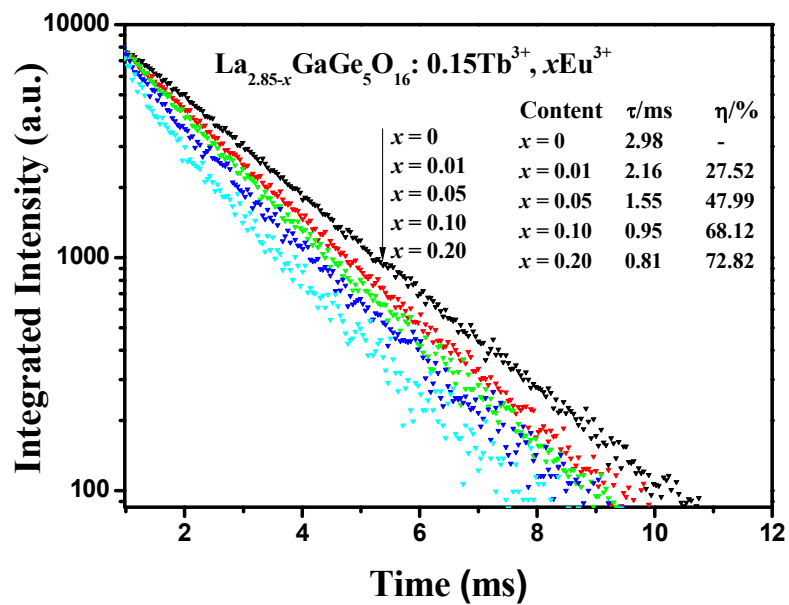


Fig. 8 Decay curves and lifetime of Tb^{3+} , and the energy transfer efficiency from Tb^{3+} to Eu^{3+} in $\text{La}_{2.85-x}\text{GaGe}_5\text{O}_{16}:0.15\text{Tb}^{3+}, x\text{Eu}^{3+}$ ($x = 0, 0.01, 0.05, 0.10, 0.20$) phosphors at room temperature.

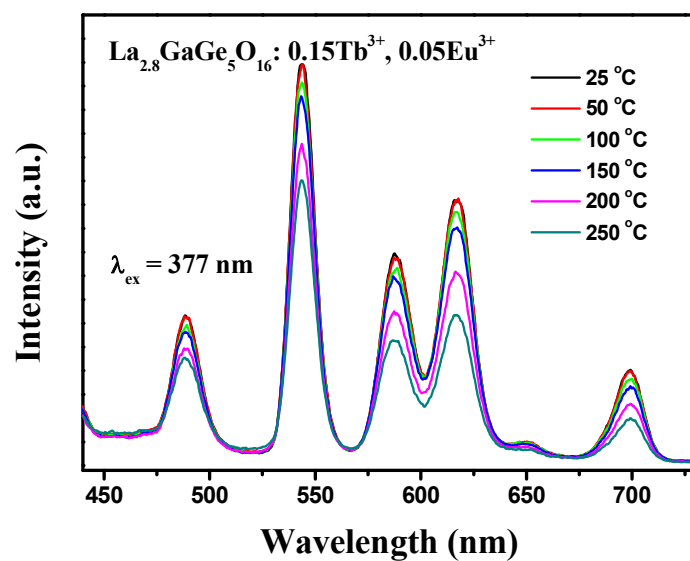


Fig. 9 Temperature-dependent PL spectra of $\text{La}_{2.8}\text{GaGe}_5\text{O}_{16}:0.15\text{Tb}^{3+}, 0.05\text{Eu}^{3+}$ under different temperatures in the range of 25-250°C.

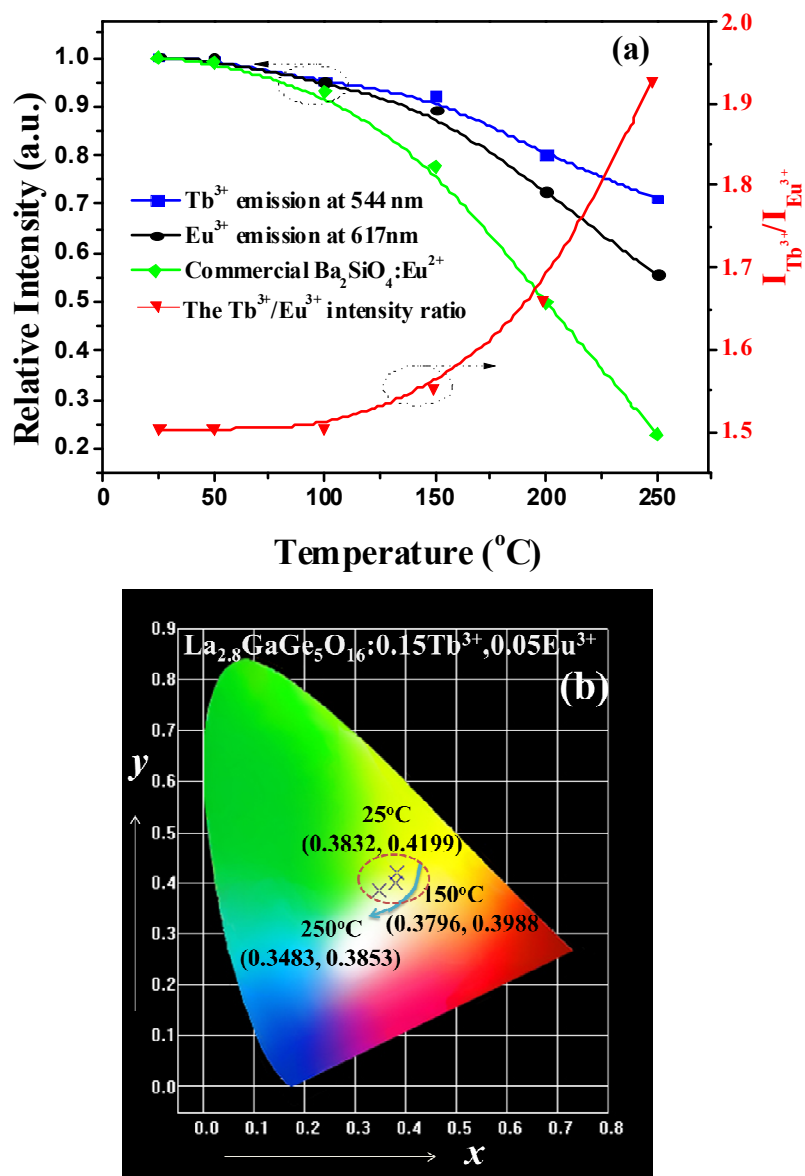


Fig. 10 The variations of the relative emission intensities (a) and CIE chromaticity coordinates (b) as a function of temperature of the $La_{2.8}GaGe_5O_{16}:0.15Tb^{3+},0.05Eu^{3+}$ phosphor.

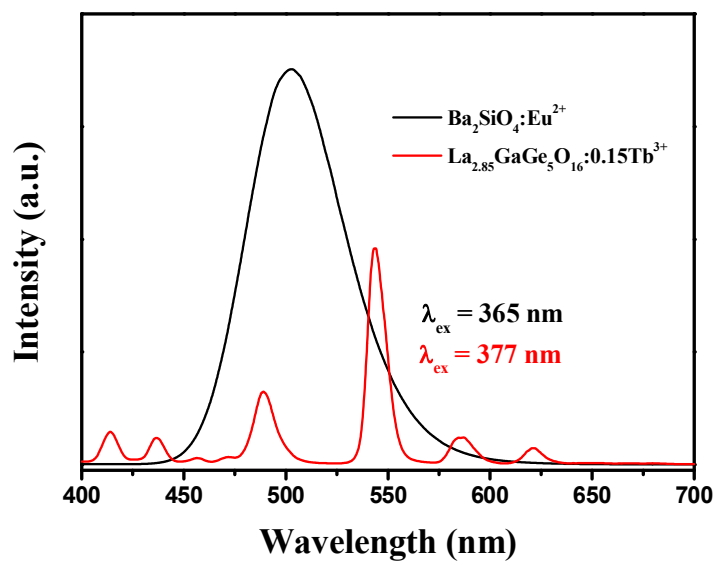


Fig. 11 PL spectra of $\text{La}_{2.85}\text{GaGe}_5\text{O}_{16}:0.15\text{Tb}^{3+}$ phosphor and commercial $\text{Ba}_2\text{SiO}_4:\text{Eu}^{2+}$ phosphors.

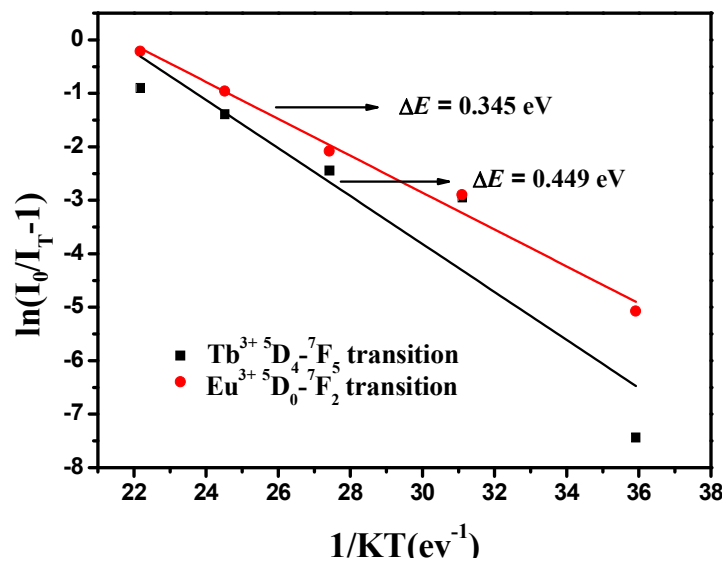


Fig. 12 A $\ln[(I_0/I_T)-1]$ vs. $1/K_B T$ activation energy graph for thermal quenching of Tb^{3+} and Eu^{3+} in $La_{2.8}GaGe_5O_{16}:0.15Tb^{3+},0.05Eu^{3+}$ phosphor.

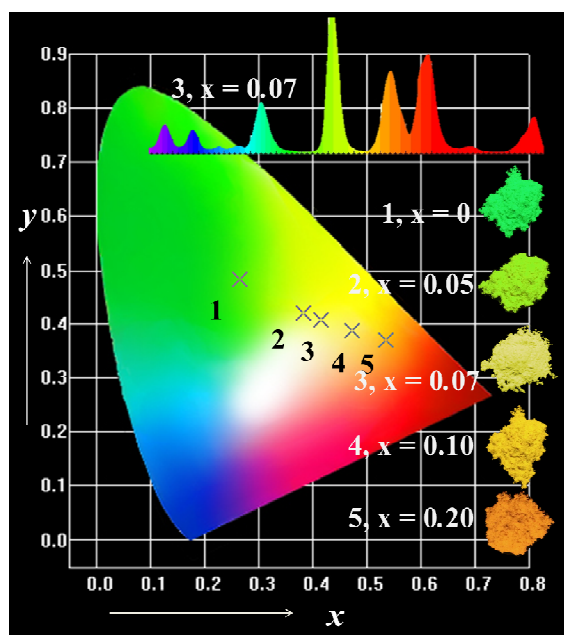


Fig. 13 CIE chromaticity diagram and a series of digital photographs of the selected of the $\text{La}_{2.85-x}\text{GaGe}_5\text{O}_{16}:0.15\text{Tb}^{3+},x\text{Eu}^{3+}$ ($x = 0, 0.05, 0.07, 0.10, 0.20$) phosphors under 377 nm excitation. The inset shows the PL spectrum of $\text{La}_{2.79}\text{GaGe}_5\text{O}_{16}:0.15\text{Tb}^{3+},0.07\text{Eu}^{3+}$ under 377nm UV light excitation.